Efficient Lithium Extraction from Shale Gas Wastewater Using Sodium Alginate/H1.33Mn1.67O4 Composite Granular Adsorbents

Efficient lithium extraction from shale gas wastewater using sodium alginate/$H_{1.33}Mn_{1.67}O_4$ composite granular adsorbents

Lun Tian [a, b], Yushun Yang [a, b], Guijing Chen [a, b], Alberto Tiraferri[c], Baicang Liu [a, b, *]

[a] College of Architecture and Environment, Institute for Disaster Management and Reconstruction, Institute of New Energy and Low-Carbon Technology, Sichuan University, Chengdu, Sichuan 610207, PR China

[b] Yibin Institute of Industrial Technology, Sichuan University Yibin Park, Section 2, Lingang Ave., Cuiping District, Yibin, Sichuan 644000, PR China

[c] Department of Environment, Land and Infrastructure Engineering, Politecnico di Torino, Corso Duca degli Abruzzi 24, 10129 Turin, Italy

[*]Corresponding author. Tel.: +86-28-85995998; fax: +86-28-62138325; E-mail: bcliu@scu.edu.cn; baicangliu@gmail.com (B. Liu).

ABSTRACT:

Dual carbon policies have spurred a rapid growth in the electric vehicle and energy storage industry, leading to a surge in demand for lithium batteries. To help meeting this demand sustainably, the natural polymer sodium alginate (SA) was crosslinked with Ca^{2+}, and the SA/HMO composite granular adsorbent was successfully prepared by crosslinking method. The aim is to extract lithium from shale gas wastewater in the Sichuan Basin, China. The produced microporous composite granular adsorbents have an average pore size of 20 nm and excellent hydrophilicity, with a swelling ratio of roughly 15 g/g at a mass concentration of 3.5 wt% alginate and 2 wt% HMO. When deployed with a real wastewater, this material achieved a lithium adsorption capacity of 4.3 mg/g. In laboratory-scale fixed bed filtration experiments, the optimal adsorbent material was saturated after approximately 700 minutes at an approach velocity (hydraulic load) of 0.47 cm/min and using total bed volume of 15 cm^3 containing approximately 0.55 g of adsorbent. In the subsequent recovery step of the adsorbed lithium through desorption, a lithium solution with concentration of 113 mg/L was achieved. The results suggest that this novel composite granular adsorbent has promising adsorption capacity and that an optimization of adsorption and desorption cycles and an engineering of the separation system deploying this material would allow high-efficiency lithium adsorption.

KEYWORDS: Lithium recovery; Composite granular adsorbent; Shale gas wastewater (SGW); Sodium alginate (SA); Hydrogen manganese oxide ($H_{1.33}Mn_{1.67}O_4$)

SYNOPSIS: The SA/HMO composite granular adsorbent prepared by crosslinking method is promising for efficient lithium recovery from shale gas wastewater.

INTRODUCTION

Lithium and its compounds possess exceptional physical and chemical properties, making them indispensable in a wide range of materials and applications, such as batteries, ceramics and glass, lubricants, air treatment, polymer processing, nuclear industry, medical, aerospace, metallurgy.[1-4] Consequently, lithium has been dubbed as "energy metal for promoting world progress" and "the white oil of the future".[5, 6] With the targets of "dual carbon" driving the rapid development of electric vehicles and energy storage industries, the demand for batteries has surged, and lithium batteries have specifically become the first choice owing to their high energy density, long service life, and relative environmental friendliness.[7, 8] It is estimated that global annual sales of electric vehicles will reach 56 million by 2040, and energy storage development will exceed 1,095 GW.[9] Therefore, it is imperative to increase the supply of lithium resources. At present, lithium resources are mainly distributed in ores, seawater and brines, such as oilfield brines, continental brines and geothermal brines.[10] Extraction of lithium from ore is complicated and will pollute the environment.[11, 12] The concentration of lithium in seawater is too low (0.17 mg/L) to be economical. Oilfield wastewater is a potential resource for recovering lithium resources.[13]

Shale gas is an unconventional natural gas resource that predominantly comprises methane. China has the world's largest reserves of shale gas, with technically recoverable resources reaching 31.6×10^{12} m^3.[14] However, the process of extracting shale gas using horizontal drilling and hydraulic fracturing techniques generates

enormous amounts of shale gas wastewater (SGW).[15, 16] The composition of SGW is complex, with high concentrations of salt, heavy metals, various organic compounds, naturally occurring radioactive materials (NORM), and many other potentially hazardous substances, posing environmental threats and technological challenges related to its treatment.[16-18] Consequently, new approaches have been proposed for SGW management that also enable the recovery of valuable elements, such as rare earth elements, uranium, and lithium, which could not only provide revenue to offset the cost of SGW treatment, but also augment the supply of strategic resources.[13, 19-21] The median concentration of lithium in SGW in the Sichuan Basin and in the Marcellus Basin is 33 mg/L and 95 mg/L,[22, 23] respectively, indicating the potential of SGW as a lithium resource. Despite these numbers, SGW remains an untapped lithium resource, and it is highly consequential to develop appropriate technology for extracting lithium from SGW.

Based on the water quality characteristics of SGW, the advantages, disadvantages and applicability of various solution lithium extraction techniques were compared. The assessed techniques include precipitation,[24] adsorption,[25, 26] electrochemical methods,[27, 28] membrane-based methods,[29, 30] and extraction.[31, 32] Adsorption method was thus considered the most appropriate technique and selected to extract lithium from SGW. In our previous studies,[33] we synthesized hydrogen manganese oxide (HMO) powder adsorbents and applied them to SGW, which showed high adsorption capacity and excellent selectivity for Li^+. However, powder cohesiveness may result in poor

flowability and difficulty in fluidization.[34] When the ratio of Mg/Li is high, Mg^{2+} in the brine is easily hydrolyzed, increasing the viscosity of the brine and reducing its pH.[35] These phenomena reduce the diffusion rate and the adsorption capacity of the adsorbent in solution.[36] In addition, during a filtration process, the powder adsorbent will lead to a large pressure drop and consequent increase in energy consumption, while the difficulty in recovering the powder adsorbent will lead to the loss of part of the powder itself.[26] The above factors limit the industrial application of powder adsorbents. In order to overcome such limitations, a number of alternative powder adsorbent forming methods have been proposed, including granulation, film forming, nanofiber, foaming. Among these, granulation is a forming method with mature technology and simple operation.

Sodium alginate (SA) is a biopolymer mainly derived from seaweed, which consists of β-D-mannuronic acid (M) and α-L-gulonic acid (G) linked by 1→4 bonds.[37] SA is rich in carboxyl and hydroxyl groups, rendering it highly hydrophilicity, non-toxic, environmentally friendly, and readily available. Thus, it is widely used as a gel agent in various industries.[38, 39] The carboxyl group in SA has an affinity for metal cations. For example, SA solutions containing divalent or multivalent metal ions may become insoluble due to the interaction of adjacent carboxyl groups with one metal ion. By using Ca^{2+} as a cross-linking agent, the SA solution can be converted into insoluble gels, described by the "egg box model".[39] In addition, the water permeability and hydrophilicity of SA have advantages when used as binder materials, because a more

permeable binder materials can reduce the overall volume of actual adsorbent that does not come into contact with SGW within the granule (vice versa, binders of poor permeability hinder the interaction of water with the adsorbent, as the latter becomes inaccessible to water due to a low-permeability isolating binder layer). Therefore, the Li^+ adsorption capacity of HMO powder adsorbent is not significantly impaired by granulation when high-permeability binders are used.[40] Therefore, SA was chosen as the crosslinking agent for the granulation of HMO powder adsorbent.

In this study, the preparation of SA/HMO composite granular adsorbent by crosslinking method is presented, and the adsorption behavior and the optimal ratio of SA and HMO powder adsorbents are discussed using adsorption kinetics and adsorption isotherms data. Under the condition of the optimal ratio of SA to HMO powder adsorbents, results of fixed bed experiments filled with SA/HMO composite granular adsorbents are evaluated, with the goal of facilitating the industrial application of lithium extraction from SGW. To better understand the physicochemical properties and adsorption behavior of the materials, we also present the outcome of a detailed material characterization, including the swelling ratio, and data obtained with SEM, XRD, and FT-IR analyses.

MATERIALS AND METHODS

MATERIALS. The SGW used in the experiments was from a shale gas well in the Lower Silurian Longmaxi Formation in Gongxian, Sichuan Basin, China, and collected in 2020.[19] The SGW samples collected prior to the experiments were stored

121 in plastic drums under dark conditions. Lithium carbonate (Li_2CO_3), manganese
122 carbonate ($MnCO_3$), hydrochloric acid (HCl), and anhydrous calcium chloride ($CaCl_2$)
123 were obtained from Kelong Chemical (Chengdu, China) and were all analytical grade.
124 Sodium alginate (SA, Lot# MKBL7997V) were obtained from MilliporeSigma (St.
125 Louis, MO, USA).
126 **Preparation of the SA/HMO composite granular adsorbents.** HMO powder
127 adsorbent was first synthesized by solid phase reaction method as described in detail in
128 our previous study.[33] Briefly, Li_2CO_3 and $MnCO_3$ were mixed in a molar ratio of
129 1.33:1.67, calcined at 500 ℃ for 4 hours, fully pickled with 0.5 mol/L HCl, and then
130 rinsed and dried several times with ultrapure water to obtain HMO powder adsorbent.
131 The HMO powder adsorbent was added into an SA solution of different concentrations
132 and stirred until evenly dispersed to form a slurry mixture. The mixture was rapidly
133 injected into 96-well enzyme labeled plates with a syringe, frozen at −20℃ for 24 hours,
134 and then freeze-dried (−50℃, < 20 Pa) for 24 hours to obtain cylindrical granules. The
135 granules were placed in 3 wt% $CaCl_2$ solution for 12 hours to complete the cross-linking
136 and rinsed 3 times with ultrapure water to remove excess $CaCl_2$ from the surface. The
137 wet adsorbent was again frozen and freeze-dried as mentioned above to obtain the final
138 dried adsorbents, which were stored in a plastic bottle for subsequent experiments. The
139 obtained composite granular adsorbents were named 3.5SA0H, 3SA2H, 3.5SA2H,
140 4SA2H according to the concentration of SA and HMO powder (**Table 1**).
141

Table 1. Composition of SA/HMO composite granular adsorbents.

	SA (wt%)	HMO (wt%)
3.5SA0H	3.5	0
3SA2H	3	2
3.5SA2H	3.5	2
4SA2H	4	2

Characterization of SA/HMO composite granular adsorbents. Power X-ray diffraction (XRD) patterns were recorded with a DX-2700 instrument (Dandong Haoyuan, China) equipped with Cu Kα radiation (k = 0.15418 nm). The adopted method was a stepwise measurement with each step angle equal to 0.05°, starting at an angle of 10° and ending at an angle of 80°. The sampling time was 0.5 s, the tube voltage and tube current were 40 kV and 30 mA, respectively. The chemical moieties of the adsorbent was analyzed with FT-IR (Spectrum Two, Perkinelmer, USA). A field-emission scanning electron microscopy (FE-SEM) (Regulus-8230, Hitachi, Japan) was used to measure the surface morphology of adsorbents. The ASAP 2460 N_2 analyzer (Micromeritics, USA) was used to determine the distribution of pore size and specific surface area of the adsorbents. The samples were degassed at 120 °C for 24 hours prior to the assay, and the sample tubes were placed in a liquid N_2 (77K) environment during the assay. The specific surface area was calculated using the Brunaue-Emmett-Teller (BET) method based on the nitrogen adsorption data, and the Barrett-Joyner-Halenda (BJH) method was used to calculate the pore size and distribution, as well as the cumulative pore volume/pore area based on nitrogen desorption data.

The swelling properties of SA/HMO composite granular adsorbent were

characterized by determining the swelling ratio. Two pieces SA/HMO composite granular adsorbent samples were immersed in 50 mL ultrapure water and left in the solution at room temperature for 24 hours. The weight of SA/HMO composite granular adsorbent before and after immersion was measured as m_d (g) and m_s (g), respectively. The swelling ratio, *S*, was calculated according to Eq. (1) :

$$S = \frac{m_d - m_s}{m_d} \quad (1)$$

Adsorption experiments. To understand whether the adsorption of lithium on the adsorbents is governed by equilibrium mechanisms and to gain insight on the adsorption capacity of the composite granular adsorbents, adsorption isotherm experiments were performed by mixing 2, 4, 7, 9, 11, or 13 pieces SA/HMO composite granular adsorbents with 30 mL of SGW. The mixture was gently stirred (200 rpm) in a shaking incubator at 25°C for 48 h to reach equilibrium. Then, the supernatant was filtered with a PES microporous membrane characterized by a pore size of 0.45 μm (Jinteng, Tianjin, China), and the concentration of lithium was measured with a PinAAcle 900T (Perkinelmer, USA). The equilibrium adsorption capacity of Li^+ was calculated according to Eq. (2).

$$q_e = \frac{(C_0 - C_e)V}{m} \quad (2)$$

where q_e (mg/g) is equilibrium adsorption capacity, V (L) is the volume of the solution, *m* (g) is the weight of SA/HMO composite granular adsorbents immerse in the solution, C_0 and C_e are the initial and equilibrium Li^+ concentrations in solution (mg/L),

respectively. To explore the adsorption mechanism, the Langmuir model (Eq. (3)), the Freundlich model (Eq. (4)), and the Temkin model (Eq. (5)) were applied, and the details are described in Text S1 (SI).

$$q_e = \frac{q_m K_L C_e}{1 + K_L C_e} \tag{3}$$

$$q_e = K_F C_e^{\frac{1}{n}} \tag{4}$$

$$q_e = B \ln(K_T \cdot C_e) \tag{5}$$

Where q_e (mg/g) and q_m (mg/g) are the equilibrium adsorption capacity and the maximum adsorption capacity, respectively. K_L (L/mg), K_F ($mg^{1-1/n} \cdot L^{1/n}/g$) and K_T (L/mg) are constants representing the affinity between adsorbents and pollutants. C_e (mg/L) is the equilibrium concentration of Li^+ and n values represents the degree of nonlinearity between solution concentration and adsorption. B is the constant related to gas constant, equilibrium binding constant, adsorption heat and absolute temperature in the Temkin model.

The dimensionless equilibrium parameter (R_L) can be calculated based on the Langmuir model according to Eq. (6). R_L is related to the adsorption characteristics, specifically, when R_L is greater than 0 and smaller than 1, the adsorption is a favorable process; when R_L is equal to 1, the adsorption is linear; when R_L is greater than 1, the adsorption is unfavorable; when R_L is equal to 0, the adsorption process is irreversible and not governed by equilibrium mechanisms[41, 42].

$$R_L = \frac{1}{1 + K_L C_0} \tag{6}$$

Adsorption kinetics experiments were performed by mixing 7 pieces SA/HMO composite granular adsorbents with 30 mL of SGW; then, the mixture was kept gently stirred (200 rpm) in a shaking incubator at 25 °C for different times (t = 1, 3, 6, 9, 12, 24, 36, 48, 60, 72 hours). The supernatant was filtered with a PES microporous membrane characterized by a pore size of 0.45 μm (Jinteng, Tianjin, China), and the concentration of lithium was measured with a PinAAcle 900T (Perkinelmer, USA). The adsorption capacity of lithium at different times was calculated as follows:

$$q_t = \frac{(C_0 - C_t)V}{m} \tag{7}$$

where q_t (mg/g) and C_t (mg/L) represent the adsorbed amount and the Li^+ concentration in solution at time t, respectively. There, V (L) is the volume of the solution, m (g) is the weight of adsorbent and C_0 is the initial lithium concentration in solution. A pseudo-first-order kinetic model (Eq. (8)), a pseudo-second-order kinetic model (Eq. (9)), and the Elovich model (Eq. (10)) were used to investigate the adsorption kinetic behaviors; the details of the models can be found in Text S2 of the Supporting Information (SI).

$$q_t = q_e \times \left(1 - \exp\left(-k_1 \cdot t\right)\right) \tag{8}$$

$$q_t = \frac{k_2 \times q_e^2 \times t}{1 + q_e \times k_2 \times t} \tag{9}$$

$$q_t = \frac{1}{\beta}\ln(\alpha\beta) + \frac{1}{\beta}\ln t \tag{10}$$

where t (h) is the adsorption time, q_e (mg/g) and q_t (mg/g) represent the equilibrium adsorption capacity and the adsorption capacity at time t, respectively. k_1 (h^{-1}) and k_2

221 ($g \cdot mg^{-1}\ h^{-1}$)) are the adsorption rate constant of the pseudo-first-order kinetic model and
222 the pseudo-second-order kinetic model, respectively. α ($mg \cdot g^{-1} \cdot min^{-1}$) and β ($g \cdot mg^{-1}$)
223 represent the initial adsorption rate and the Elovich model adsorption constant.

224 An adsorption selectivity test was performed by mixing 7 pieces SA/HMO
225 composite granular adsorbents with 30 mL of SGW and the mixture was gently stirred
226 (200 rpm) in a shaking incubator at 25°C for 48 hours. The supernatant was filtered
227 with a PES microporous membrane characterized by pore size of 0.45 μm (Jinteng,
228 Tianjin, China) to measure the metal ion concentration using a Dionex Integrion HPIC
229 (Thermo Fisher, USA). The partition coefficient (K_d, Eq. (11)), concentration factor
230 (CF, Eq. (12)), and separation factors (α_{Me}^{Li}, Eq. (13)) were calculated to investigate the
231 adsorption selectivity of SA/HMO adsorbents, as follows:

232 $$K_d = \frac{C_0 - C_e}{C_e} \times \frac{V}{m} \tag{11}$$

233 $$CF = \frac{q_e(Me)}{C_0(Me)} \tag{12}$$

234 $$\alpha_{Me}^{Li} = \frac{K_d(Li)}{K_d(Me)} \tag{13}$$

235 where Me refer to a metal ion, namely, Li^+, Na^+, K^+, Mg^{2+}, Ba^{2+}, Sr^{2+}. In the equations
236 above, $q_e(Me)$ (mg/g) represents the equilibrium adsorption capacity, C_0 and C_e
237 are the initial and equilibrium Me concentrations in solution (mg/L), respectively, V (L)
238 is the volume of the solution, and m (g) is the weight of SA/HMO composite granular
239 adsorbents.

240 **Fixed bed filtration experiments.** The fixed bed adsorption experimental device

241 is shown in **Figure S1** of the SI. The adsorbent bed was obtained by filling a glass sand
242 core chromatography column with 3.5SA2H composite granular adsorbents. An
243 appropriate amount of glass beads of suitable size was placed above the adsorbent to
244 prevent the adsorbent from floating. The continuous water inlet and continuous water
245 outlet were adopted with the upward flow direction under fully saturated conditions.
246 The specific operating parameters of the bed filtration are summarized in **Table 2**. After
247 different running times, the concentration of Li^+ in the effluent of the bed was measured
248 with a PinAAcle 900T (Perkinelmer, USA).

249 **Table 2.** Fixed bed filtration operating parameters.

Pump speed (r/min)	Flow rate (mL/min)	EBCT (min)	Adsorbent weight (g)	Fixed bed diameter (cm)	Fixed bed length (cm)	Empty bed volume (cm^3)	Approach velocity (cm/min)
0.5	0.269	55	0.547	1	19	14.92	0.34
0.7	0.366	40	0.5432	1	19	14.92	0.47
1	0.545	27	0.5385	1	19	14.92	0.70

250

251 **RESULTS AND DISCUSSION**

252 **Physico-chemical characteristics of SA/HMO composite granular adsorbents.**
253 **Figure 1a** shows representative XRD patterns of HMO alone, 3.5SA0H (only sodium
254 alginate), 3SA2H, 3.5SA2H, 4SA2H. Two broad peaks of low intensity can be seen for
255 the alginate material, 3.5SA0H, near 2θ=20° and 40°. The three main characteristic
256 peaks of the HMO powder are instead 19.1°, 37°, 45.05°, and the corresponding crystal
257 face distances are 4.643 Å, 2.428 Å, 2.011 Å, respectively. The three main characteristic
258 peaks of the XRD patterns of the composite materials, namely, 3SA2H, 3.5SA2H and

4SA2H, are around 19.7°, 37.45° and 45.3°, and the corresponding crystal face distances are 4.503 Å, 2.399 Å and 2.000 Å, respectively, indicating that HMO powder was successfully loaded within the alginate matrix. Compared with pure HMO powder, the peak positions of SA/HMO composite granular adsorbents shifted to larger angle and this shift increased with higher sodium alginate content. Also, the presence of sodium alginate also corresponded to a reduction of the peak intensity, which was associated with the two wide peaks characterizing the pure alginate sample, 3.5SA0H. **Figure 1b** presents representative FT-IR spectra of 3.5SA (not cross-linked pure SA), 3.5SA0H, 3SA2H, 3.5SA2H, and 4SA2H. There are four typical absorption bands at 3243, 1590, 1416, and 1026 cm^{-1}, corresponding to the functional groups O-H, C=O, C-OH, and OC-OH.[39] Compared with 3.5SA, 3.5SA0H showed a new absorption band at 2852 cm^{-1}, which may be related to the C-H stretch vibration caused by the reaction of SA polymerization chain with Ca^{2+}, thus suggesting appropriate cross-linking of the sample.[38]

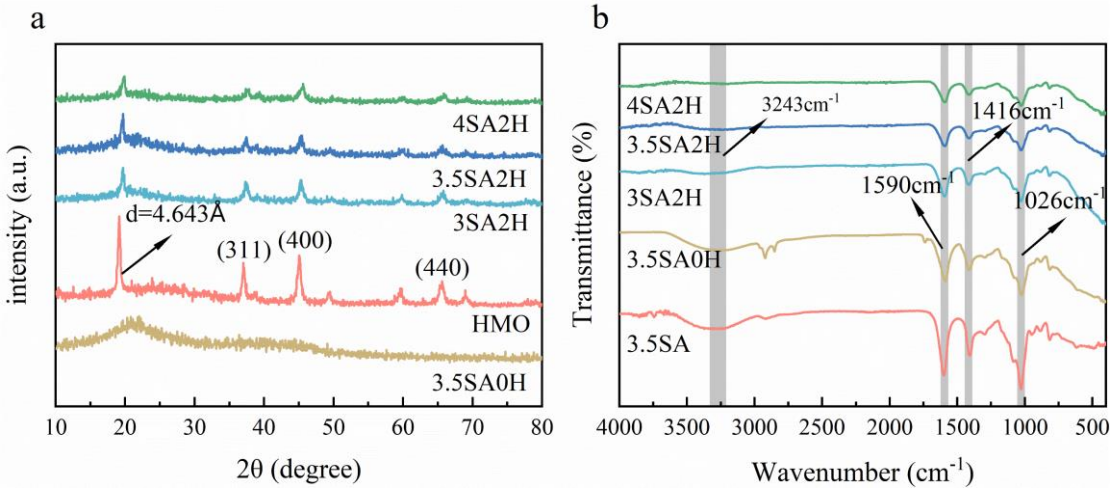

Figure 1. (a) XRD patterns of various samples, including cross-linked alginate

(3.5SA0H), pure adsorbent powder (HMO), composite granular adsorbent (3SA2H, 3.5SA2H, 4SA2H). (b) FT-IR spectra of not cross-linked alginate (3.5SA) and the same samples analyzed with XRD.

Figure S2 (SI) presents representative SEM micrographs of 3.5SA2H composite granular adsorbent before and after its use for adsorption. The SA/HMO composite granular adsorbent had a three-dimensional porous structure, which is conducive to swelling and diffusion of Li^+ into the gel.[43] **Figure 2a** shows the nitrogen adsorption-desorption isotherms of 3SA2H, 3.5SA2H, and 4SA2H composite granular adsorbents, all of which are typical type IV isotherms with H3 hysteresis loop.[44] This behavior is similar to the nitrogen adsorption-desorption isotherm of the HMO powder,[33] again corroborating the conclusion that the HMO powder was successfully loaded into the granule. Specifically, the nitrogen adsorption capacities of 3SA2H, 3.5SA2H, and 4SA2H were 18.9, 24.8, and 20.1 cm^3/g (STP), respectively. The BJH method was applied to calculate the pore size distribution of desorption branches of nitrogen adsorption-desorption isotherm, and the results are shown in **Figure 2b**. The average pore diameter of the three adsorbents was about 20 nm. **Figure 2c** is the superposition diagram of the cumulative pore volume and pore area as a function of pore size: the cumulative pore volume of 3SA2H, 3.5SA2H, and 4SA2H was 0.032, 0.04, 0.034 cm^3/g, respectively, and the cumulative pore area was 14.4, 18.8, 17.8 m^2/g, respectively. Finally, **Figure 2d** shows the BET surface area plot drawn as a function of relative

pressure of the isothermal adsorption branch with values in the range 0.07-0.26: the resulting BET surface area of 3SA2H, 3.5SA2H, and 4SA2H was estimated as 8.95, 13.79 and 11.82 m^2/g, respectively. Overall, the nitrogen adsorption capacity and surface areas were the highest for the 3.5SA2H adsorbent.

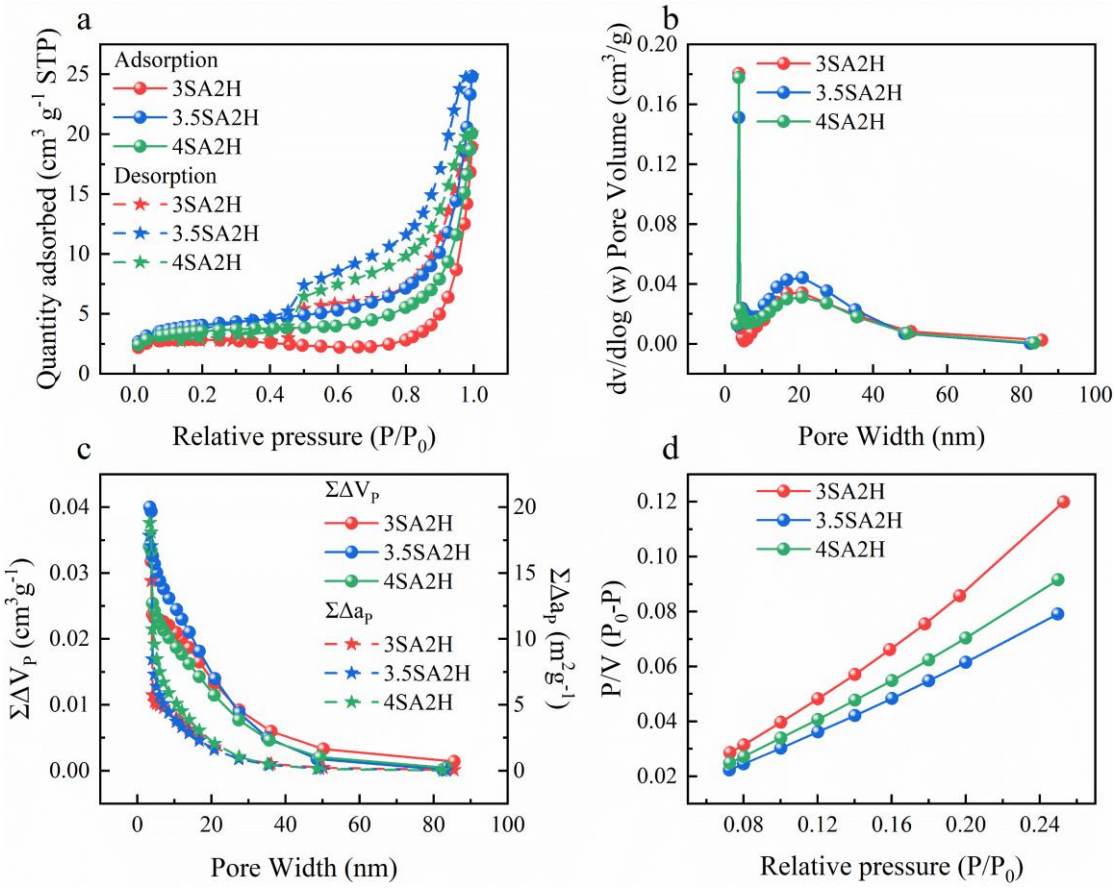

Figure 2. (a) Nitrogen adsorption-desorption isotherm diagram of three SA/HMO composite granular adsorbents. (b) Pore size distribution diagram. (c) Cumulative pore volume and pore area distribution. (d) BET specific surface area diagram.

Swelling behavior of SA/HMO composite granular adsorbents. Swelling is a physicochemical phenomenon that has been studied to explain the behavior and properties of hydrogels.[45] Excellent swelling behavior is typically conducive to the

adsorption of heavy metal ions.[43] The SA/HMO composite granular adsorbents possess remarkable water-clearing properties, swiftly absorbing water molecules and causing them to swell. The alteration in the water contact angle, reflecting the super hydrophilic nature of 3.5SA2H, is depicted in **Movie S1**. The calculated swelling ratios of the SA/HMO composite granular adsorbents are shown in **Figure 3a**. The ratio obtained for 3SA2H was as high as 18.8 g/g, indicating its excellent swelling property, which is attributed to its three-dimensional pore structure and the abundant hydrophilic groups on the sodium alginate polymer chain. Note that the swelling ratio of alginate-only 3.5SA0H was greater than that of the composite 3.5SA2H sample, due in part to the increase of dry weight caused by the addition of HMO powder adsorbent and in part to the fact that the water absorption performance of HMO powder adsorbent itself is much lower than that of sodium alginate. Interestingly, when comparing 3SA2H, 3.5SA2H, and 4SA2H samples under normalized mass concentration of HMO powder adsorbent, the swelling ratio slightly decreased with the increase of sodium alginate amount. This fact is attributed to the fact that the pore size of the composite granular adsorbent was smaller with increased alginate, and to the fact that the dry weight increased. However, the swelling ratio of 4SA2H was 12.3 g/g, indicating that the composite granular adsorbents prepared by the method described above had excellent swelling performance regardless of the amount of alginate, providing valuable conditions for interactions with water, and consequently high potential for adsorption of lithium.

Effect of adsorbent dose on Li^+ adsorption. The extraction of lithium from SGW with different adsorbent dosages was investigated, and the results are summarized in **Figure 3b**. Indeed, the dosage had a significant impact on the lithium recovery rate and adsorption capacity. Specifically, the recovery rate gradually increased with dosage, but the adsorption capacity gradually decreased. Taking 3.5SA2H as an example, when the dosage increased from 1.1 g/L to 6.9 g/L, the recovery rate of lithium increased from 15.7% to 86.7%, while the adsorption capacity decreased from 4.31 mg/g to 3.87 mg/g. The increase in recovery rate is associated with an increase in total adsorption sites that can capture more Li^+. The high lithium recovery rate achieved under the condition of relatively low dosage of adsorbent indicates that the adsorbent has excellent affinity for lithium extraction.[46] The adsorption capacity decreased with increasing adsorbent dosage likely due overdosing of the adsorbent, which translates into a smaller amount of lithium adsorbed per unit mass of adsorbent and to the lower kinetics of adsorption during the process, as more lithium passed into solid phase (and less remained in solution) compared to the case at lower adsorbent dosage. Therefore, although the removal rate was higher at higher dosage, the actual utilization of adsorbent was less efficient, because of underconsumption of available adsorption site, pointing to the fact that there is an engineering trade-off that needs consideration to simultaneously maximize absolute lithium adsorption while minimizing the amount of required adsorbent. Simply comparing the various composite granular adsorbents at the same dosage, one can conclude that the adsorption capacity and recovery rate of 3.5SA2H

was the largest, and that of 3SA2H was the smallest.

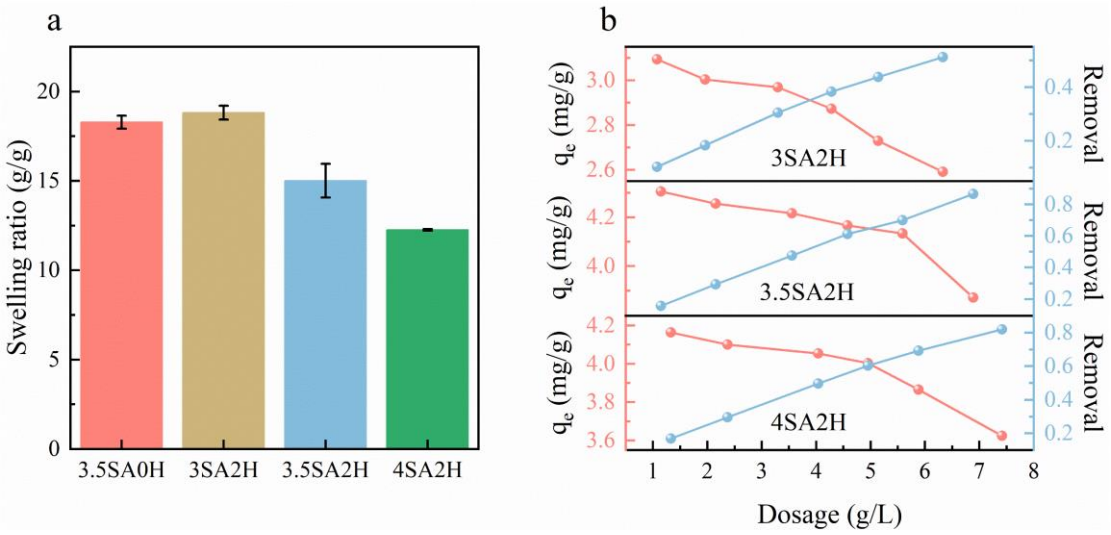

Figure 3. (a) Swelling ratio of composite granular adsorbents prepared with different sodium alginate amount. (b) Influence of the dosage on the adsorption capacity and removal rate of lithium in SGW with three composite granular adsorbents.

Adsorption isotherms of lithium onto SA/HMO composite granular adsorbents**.** Adsorption isotherm and the respective fitting models are presented in **Figure 4a-c**. The data suggests that a saturation condition existed for the adsorbents, as the adsorption capacity was only slightly higher when in equilibrium with larger liquid concentration above a certain value. The maximum adsorption capacities obtained in the experiments for 3SA2H, 3.5SA2H, and 4SA2H were 3.09 mg/g, 4.31 mg/g, and 4.16 mg/g respectively, which can be converted to 7.73 mg/g HMO, 11.85 mg/g HMO and 12.48 mg/g HMO respectively. Compared with the adsorption capacity of HMO powder adsorbents for lithium (13.27 mg/g) in shale gas wastewater, the adsorption efficiency of 3SA2H,3.5SA2H and 4SA2H composite granular adsorbents is 58.2%, 89.3%,

366 94.0%, respectively, which is superior to the literature adsorbents presented in Table S1.
367 This order was consistent with the results of nitrogen adsorption, indicating that a higher
368 BET surface area was correlated to a better adsorption of Li^+. The value of fitting
369 coefficient, R^2, was highest for the Langmuir model, corroborating the observation of a
370 saturation condition and suggesting that the adsorption of Li^+ was akin to that of a
371 monolayer chemisorption process that occurs at specific homogeneous sites on the
372 surface of SA/HMO.[47] Also, the data suggests that there was no obvious competition
373 between solvent and sorbate to occupy the adsorption sites.[48] This result was analogous
374 to the adsorption behavior of pure HMO powder adsorbent, indicating that granulation
375 by polymer sodium alginate did not significantly change the adsorption mechanism.
376 The separation factor R_L calculated with the equilibrium coefficient K_L of the Langmuir
377 model was 0.207, 0.027 and 0.034, respectively, for 3SA2H, 3.5SA2H and 4SA2H
378 samples. Being between 0 and 1, adsorption can be described as favorable, also
379 suggested by the *n* parameters of the Freundlich model being greater than 1.[49] Note that
380 the fact that the parameter was relatively close to 0 possibly suggests that the adsorption
381 was not entirely, or quickly, reversible, and that equilibrium models may not be
382 completely adequate to describe the adsorption/desorption phenomena and /or that
383 desorption kinetics are significantly slower than adsorption kinetics. This fact would
384 pose a challenge when attempting to extract and recover (load and unload) lithium with
385 the adsorbents, further suggesting the need for an engineering optimization of a
386 potential system deploying these materials.

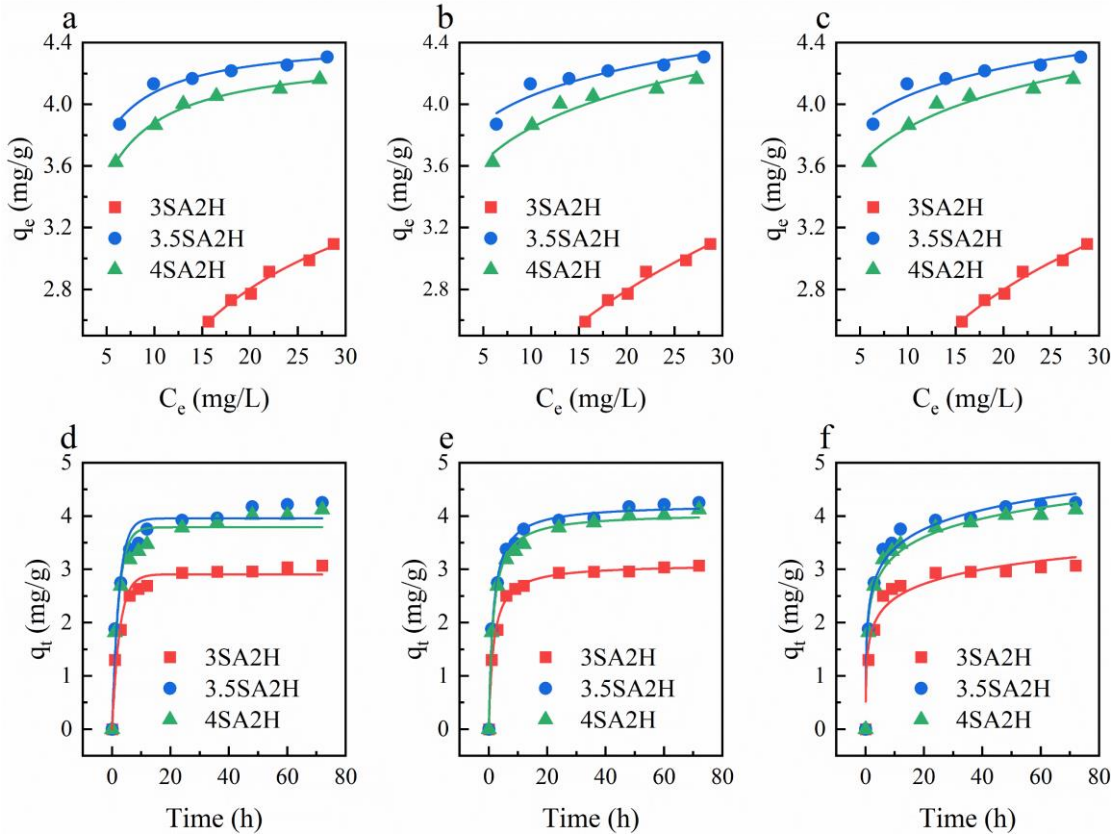

Figure 4. Adsorption isotherms of lithium with three different composite granular adsorbents fitted with the (a) Langmuir model, (b) Freundlich model, and (c) Temkin model. Adsorption kinetics fitted with a (d) pseudo-first-order kinetic model, (e) pseudo-second-order kinetic model, and (f) Elovich model.

Table 3. Fitting parameters from adsorption isotherm models.

	Parameters	3SA2H	3.5SA2H	4SA2H
Langmuir	Q_m (mg/g)	3.98	4.43	4.33
	K_L (L/mg)	0.120	1.16	0.863
	R^2	0.980	0.960	0.992
Freundlich	K_F ($mg^{1-1/n} \cdot L^{1/n}/g$)	1.25	3.51	3.16
	n	3.56	16.0	11.6
	R^2	0.977	0.888	0.940
Temkin	B	0.802	0.260	0.341
	K_T (L/mg)	1.64	608	792
	R^2	0.979	0.895	0.949

Adsorption kinetics of lithium onto SA/HMO composite granular adsorbents**.** Kinetics data and model results are shown in **Figure 4d-f**, while the resulting fitting parameters are summarized in **Table 4**. Generally, the adsorption was faster during the first 6 hours of the tests, then the rate decreased and ceased after roughly 48 hours. The main reason is that the number of readily available adsorption sites on the SA/HMO surface decreased with time. In later stages of the test, the adsorption of Li^+ is controlled by diffusion into the smaller pores of the adsorbent, significantly reducing the kinetics, until all the available adsorption sites within the timescale of the experiments were consumed.[49] The adsorption capacity calculated from the kinetics data by the pseudo-second-order kinetic model was in better agreement with the experimental results with respect to other models, and was also consistent with the isotherms data. Additionally, the correlation coefficient R^2 for the pseudo-second-order kinetic model was also the largest among the three models, which suggests that chemisorption is the rate limiting step for Li^+ adsorption.[50] This conclusion is the same as observed in the adsorption process with pure HMO, once again indicating that granulation did not change the adsorption mechanism or capability of the powder.

411 **Table 4.** Parameters from data fitting with kinetics models.

	Parameters	3SA2H	3.5SA2H	4SA2H
Pseudo-first	$q_{e,cal}$ (mg/g)	2.91	3.96	3.79
	k_1 (min^{-1})	0.383	0.434	0.443
	R^2	0.969	0.957	0.949
Pseudo-second	$q_{e,cal}$ (mg/g)	3.10	4.22	4.05
	k_2 (g/(mg.h))	0.201	0.162	0.168
	R^2	0.995	0.994	0.993
Elovich	α (mg/g/min)	20.3	35.2	32.2
	β (g/mg)	2.55	1.92	1.98
	R^2	0.969	0.981	0.987

412

413 **Adsorption selectivity of lithium by 3.5SA2H adsorbent in SGW.** SGW
414 contains substantial amounts of Na^+, K^+, Mg^{2+}, Ba^{2+}, Sr^{2+}, which are the main
415 competition ions potentially limiting lithium extraction. The 3.5SA2H composite
416 granular adsorbent had a high selectivity for Li^+, and the results of selectivity
417 experiments are summarized in **Table 5**. The partition coefficients of the cations were
418 ordered as $Li^+ > Ba^{2+} > Sr^{2+} > Mg^{2+} > K^+ > Na^+$. In addition, the separation factors
419 estimated for Li^+, namely, 1.21, 3.84, 23.85, 24.86, 27.52 for Ba^{2+}, Sr^{2+}, Mg^{2+}, K^+, and
420 Na^+, respectively, corroborated that Li^+ was preferentially adsorbed onto 3.5SA2H[51]
421 and that Ba^{2+} is the cation posing the larger potential competition to adsorption. The
422 adsorption capacity of the SA/HMO composite granular adsorbent for Li^+ is mainly
423 determined by the HMO component. The high selectivity for Li^+ is rationalized with
424 the ion sieve effect of HMO: the spinel structure size is suitable for Li^+, and suitable
425 ion exchange occurs between H^+ and Li^+. According to this rationalization, other metal
426 ions can only be adsorbed on the surface by van der Waals force because their ionic

427 radius is larger than the adsorption site/cavity size and/or because the free energy of
428 hydration is larger than Li^+, which prevents their entry into the HMO cavity site.[52, 53]

429

430 **Table 5.** Adsorption selectivity of lithium by 3.5SA2H sample in the SGW

	C_0 (mg/L)	C_e (mg/L)	q_e (mg/g)	K_d (ml/g)	CF (ml/g)	α_{Me}^{Li}
Li^+	32.9	17.6	4.05	231	123	1.00
Na^+	11000	10700	89.2	8.38	8.08	27.5
K^+	266	257	2.38	9.28	8.97	24.9
Ba^{2+}	110	64.2	16.5	190	150	1.21
Sr^{2+}	105	85.8	5.15	60.0	49.0	3.84
Mg^{2+}	74.9	72.2	0.700	9.67	9.33	23.9

431

432 **Results of lithium extraction and recovery in preliminary depth filtration**
433 **experiments.** The empty bed contact time (EBCT) is an important parameter related to
434 the reactor volume size or to the flow rate processable in a system and should be as
435 small as possible to ensure economy of the process. Indeed, decreasing EBCT may
436 reduce the efficacy of lithium extraction if the timescales of solution flow in the
437 granular bed are too high with respect to the kinetics of partition between the liquid and
438 the solid phase (adsorption). In this study, various EBCT values were investigated in
439 preliminary filtration tests. **Figure 5a** presents the performance of lithium recovery
440 observed for the 3.5SA2H composite granular adsorbent in SGW. The adsorbent
441 depletion time (C/C_0=0.95) was 1100, 703, and 543 minutes for different and increasing
442 flow rates. The initial effluent (recovered) lithium concentration was high regardless of
443 the flow rate, and then rapidly decreased approaching 0. Specifically, the initial effluent

lithium concentration was as high as 113 mg/L at an approach velocity of roughly 0.7 cm/min, indicating that reasonable control of the desorption time can achieve a lithium-rich solution. Indeed, the optimization of the filtration conditions is outside the scope of this study, but it is crucial to optimize adsorbent utilization as well as lithium extraction and recovery.

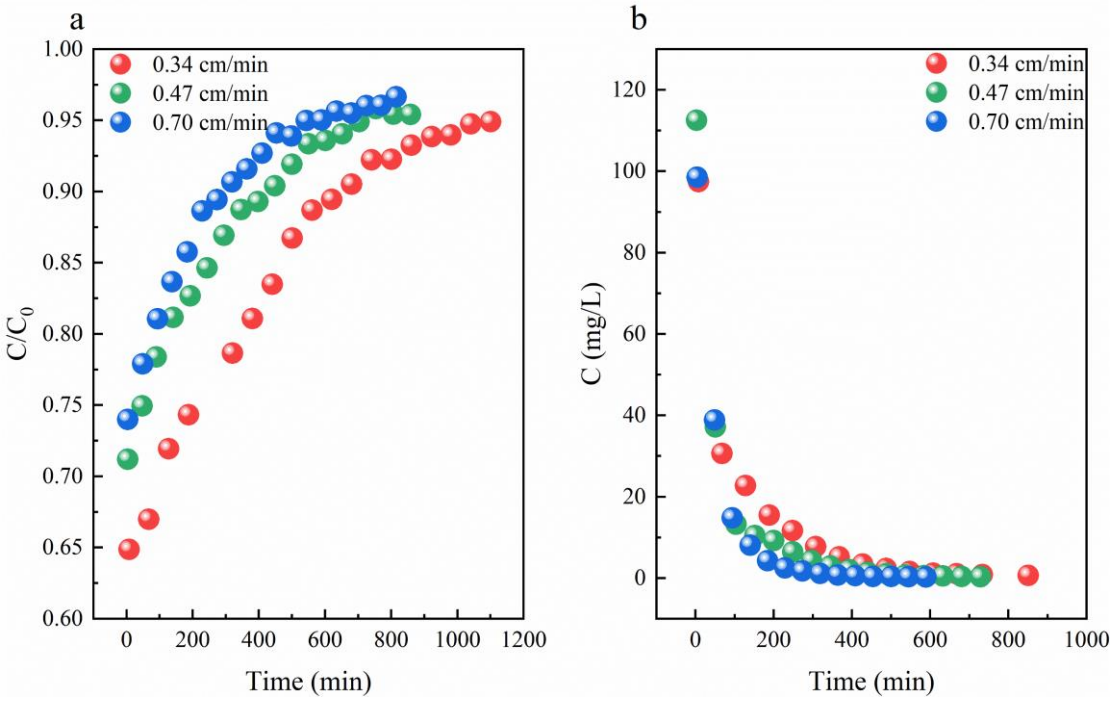

Figure 5. (a) Changes of residual lithium ratio in effluent with time under adsorption at different approach velocity values through a fixed bed. (b) Changes of lithium concentration in the effluent with time under different approach velocity conditions.

CONCLUSION

To overcome the practical limitations of the use of HMO powder adsorbents for lithium extraction, SA/HMO composite granular adsorbents with three-dimensional network structure were proposed, prepared by crosslinking method using SA as

crosslinking agent, and evaluated for lithium adsorption in SGW. The SA/HMO was a mesoporous material with an average pore size of 20 nm and had excellent hydrophilicity with a swelling ratio of up to 15 g/g for a specific optimal combination of sodium alginate and HMO powder amounts, namely, for sample referred to as 3.5SA2H. When the dosage of 3.5SA2H was 6.9 g/L, the recovery rate of lithium was 86.7%, and the adsorption capacity was 3.87 mg/g. The adsorption kinetics and adsorption isotherm experiments suggested that the adsorption process of SA/HMO in SGW could be adequately described by a pseudo-second-order kinetic model and by a Langmuir saturation model, suggesting that the adsorption process was akin to a monolayer chemisorption and that the adsorption rate was likely controlled by the chemisorption step. Consequentially, the composite granular adsorbent had high selectivity for lithium and its behavior was analogous to that of a pure HMO powder, indicating that the incorporation of HMO within a sodium alginate granule did not reduce the capability of the adsorbent material and that the granule configuration is therefore superior to the pure powder, as the former provides significant gains toward the practical implementation of the technology. The results of preliminary fixed-bed filtration experiments consisting of SGW flowing through a column filled with 3.5SA2H suggested that this material has high potential for use in the extraction and recovery of lithium from complex aqueous matrices. In particular, the recovered lithium concentration during the desorption step reached 112.5 mg/L: further engineering of the system would significantly increase the efficacy of lithium recovery and the utilization

efficiency of the adsorbent. This study demonstrates that SA/HMO composite granular adsorbent has practical application value in extracting lithium from SGW.

ASSOCIATED CONTENT

Supporting Information

The Supporting Information is available free of charge online.

Adsorption isotherm models (Text S1); Adsorption kinetic models (Text S2); Fixed bed experimental setup diagram (Figure S1); SEM micrographs (Figure S2); Water contact angle of 3.5SA2H (Movie S1) and compassion of Li^+ uptake properties (Table S1).

AUTHOR INFORMATION

Corresponding Author

Baicang Liu − College of Architecture and Environment, Institute for Disaster Management and Reconstruction, Institute of New Energy and Low-Carbon Technology, Sichuan University, Chengdu, Sichuan 610207, People's Republic of China; Yibin Institute ofIndustrial Technology, Sichuan University, Yibin, Sichuan 644000, People's Republic of China; orcid.org/0000-0003-3219-1924; Phone: +86-28-85995998; Email: bcliu@scu.edu.cn, baicangliu@gmail.com; Fax: +86-28-62138325

Authors

Lun Tian − College of Architecture and Environment, Institute for Disaster Management and Reconstruction, Institute of New Energy and Low-Carbon Technology, Sichuan University, Chengdu, Sichuan 610207, People's Republic of

China; Yibin Institute ofIndustrial Technology, Sichuan University, Yibin, Sichuan 644000, People's Republic of China

Yushun Yang − College of Architecture and Environment, Institute for Disaster Management and Reconstruction, Institute of New Energy and Low-Carbon Technology, Sichuan University, Chengdu, Sichuan 610207, People's Republic of China; Yibin Institute ofIndustrial Technology, Sichuan University, Yibin, Sichuan 644000, People's Republic of China

Guijing Chen − College of Architecture and Environment, Institute for Disaster Management and Reconstruction, Institute of New Energy and Low-Carbon Technology, Sichuan University, Chengdu, Sichuan 610207, People's Republic of China; Yibin Institute ofIndustrial Technology, Sichuan University, Yibin, Sichuan 644000, People's Republic of China

Alberto Tiraferri − Department of Environment, Land and Infrastructure Engineering, Politecnico di Torino, Corso Duca degli Abruzzi 24, 10129 Turin, Italy; orcid.org/0000-0001-9859-1328

ACKNOWLEDGMENTS

This work was supported by the National Natural Science Foundation of China (52270075, 52070134), Litree Purifying Technology Co., Ltd. Project (2021H012), and Sichuan University and Yibin City People's Government strategic cooperation project (2020CDYB-2). A.T. acknowledges the MICS (Made in Italy – Circular and Sustainable) Extended Partnership and funding from the European Union Next-

GenerationEU (Piano Nazionale di Ripresa e Resilienza (PNRR) – Missione 4 Componente 2, Investimento 1.3 – D.D. 1551.11-10-2022, PE00000004). This manuscript reflects only the authors' views and opinions, none of the funding agencies can be considered responsible for them.

REFERENCES

1. U.S., G. S. *Mineral commodity summaries 2022: U.S. Geological Survey*; 2022; 2022; p 202.
2. Draaisma, D., Lithium: the gripping history of a psychiatric success story. *Nature* **2019,** *572* (7771), 584-585.
3. Sun, Y.; Wang, Q.; Wang, Y.; Yun, R.; Xiang, X., Recent advances in magnesium/lithium separation and lithium extraction technologies from salt lake brine. *Separation and Purification Technology* **2021,** *256*, 117807.
4. Zhang, S.; Wang, Z.; Chen, C.; Jia, J.; Chen, Z., Pressure wave behavior and its effects on structure under In-box LOCA in a helium-cooled lead lithium blanket of hydrogen fusion reactors. *International Journal of Hydrogen Energy* **2021,** *46* (10), 7415-7425.
5. Zhang, G.; Zhang, J.; Zhou, Y.; Qi, G.; Zeng, J.; Sun, Y.; Shen, Y.; Li, X.; Ren, X.; Dong, S.; Sun, C.; Wu, Z.; Hai, C.; Tang, W., Practical synthesis of manganese oxide MnO2·0.5H2O for an advanced and applicable lithium ion-sieve. *Journal of Solid State Chemistry* **2021,** *293*.
6. Zhang, X.; Li, Z.; Liu, J.; Xu, F.; Zheng, L.; Wolfc, S. D.; Lai, Z.; Lu, X., Solar-driven ultrafast lithium extraction from low-grade brine using microfluidics-mediated vortex in scalable electrochemical reactors. *Chemical Engineering Journal* **2023,** *454*, 140074.
7. Scrosati, B.; Hassounab, J.; Sun, Y.-K., Lithium-ion batteries. A look into the future. *Energy & Environmental Science* **2011,** *4* (9), 3287-3295.
8. Xie, J.; Lu, Y.-C., A retrospective on lithium-ion batteries. *Nature Communications* **2020,** *11* (1), 2499.
9. He, X.; Kaur, S.; Kostecki, R., Mining Lithium from Seawater. *Joule* **2020,** *4* (7), 1357-1358.
10. Swain, B., Recovery and recycling of lithium: A review. *Separation and Purification Technology* **2017,** *172*, 388-403.
11. Hou, J.; Zhang, H.; Thornton, A. W.; Hill, A. J.; Wang, H.; Konstas, K., Lithium Extraction by Emerging Metal‐Organic Framework‐Based Membranes. *Advanced Functional Materials* **2021,** *31* (46), 2105991.
12. Yang, S.; Zhang, F.; Ding, H.; He, P.; Zhou, H., Lithium Metal Extraction from Seawater. *Joule* **2018,** *2* (9), 1648-1651.
13. Kumar, A.; Fukuda, H.; Hatton, T. A.; John H. Lienhard, V., Lithium Recovery from Oil and Gas Produced Water: A Need for a Growing Energy Industry. *ACS Energy Letters* **2019,** *4* (6), 1471-1474.
14. Cui, W.; Liu, J.; Ji, Z.; Guo, X.; Li, F.; Zhao, Y.; Wang, S.; Yuan, J., Typical organic fouling in the electrodialysis concentration/desalination process of shale gas fracturing flowback water. *Environmental Science Water Research & Technology* **2022,** *8* (10), 2254-2264.
15. Tang, P.; Xie, W.; Tian, L.; Tan, B.; Zhang, Y.; Yang, Z.; Chen, C.;

Zhang, W.; Liu, B., Oxidation-biotreatment-membrane combined process for external reuse of shale gas wastewater. *Separation and Purification Technology* **2022,** *291*, 120920.
16. Liu, Y.; An, N.; Tian, L.; Yang, P.; Wang, W.; Liu, B., Multifunctional carbon aerogel granules designed for column reactor for efficient treatment of shale gas flowback and produced water. *Chemical Engineering Journal* **2023,** *459*, 141544.
17. Tang, P.; Xie, W.; Tiraferri, A.; Zhang, Y.; Zhu, J.; Li, J.; Lin, D.; Crittenden, J. C.; Liu, B., Organics removal from shale gas wastewater by pre-oxidation combined with biologically active filtration. *Water Research* **2021,** *196*, 117041.
18. Xie, W.; Tian, L.; Tang, P.; Cui, J.; Wang, T.; Zhu, Y.; Bai, Y.; Tiraferri, A.; Crittenden, J. C.; Liu, B., Shale gas wastewater characterization: Comprehensive detection, evaluation of valuable metals, and environmental risks of heavy metals and radionuclides. *Water Research* **2022,** *220*, 118703.
19. Tian, L.; Chang, H.; Tang, P.; Li, T.; Zhang, X.; Liu, S.; He, Q.; Wang, T.; Yang, J.; Bai, Y.; Vidic, R. D.; Crittenden, J. C.; Liu, B., Rare Earth Elements Occurrence and Economical Recovery Strategy from Shale Gas Wastewater in the Sichuan Basin, China. *ACS Sustainable Chemistry & Engineering* **2020,** *8* (32), 11914-11920.
20. Robbins, C. A.; Du, X.; Bradley, T. H.; Quinn, J. C.; Bandhauer, T. M.; Conrad, S. A.; Carlson, K. H.; Tong, T., Beyond treatment technology: Understanding motivations and barriers for wastewater treatment and reuse in unconventional energy production. *Resources, Conservation & Recycling* **2022,** *178*, 106011.
21. Chang, H.; Liu, B.; Crittenden, J. C.; Vidic, R. D., Resource Recovery and Reuse for Hydraulic Fracturing Wastewater in Unconventional Shale Gas and Oil Extraction. *Environmental Science & Technology* **2019,** *53* (23), 13547-13548.
22. Haluszczak, L. O.; Rose, A. W.; Kump, L. R., Geochemical evaluation of flowback brine from Marcellus gas wells in Pennsylvania, USA. *Applied Geochemistry* **2013,** *28*, 55-61.
23. Xie, W.; Tang, P.; Wu, Q.; Chen, C.; Song, Z.; Li, T.; Bai, Y.; Lin, S.; Tiraferri, A.; Liu, B., Solar-driven desalination and resource recovery of shale gas wastewater by on-site interfacial evaporation. *Chemical Engineering Journal* **2022,** *428*, 132624.
24. Zhang, Y.; Hua, Y.; Wang, L.; Sun, W., Systematic review of lithium extraction from salt-lake brines via precipitation approaches. *Minerals Engineering* **2019,** *139*, 105868.
25. Safari, S.; Lottermoser, B. G.; Alessi, D. S., Metal oxide sorbents for the sustainable recovery of lithium from unconventional resources. *Applied Materials Today* **2020,** *19*, 100638.
26. Xu, X.; Chen, Y.; Wan, P.; Gasem, K.; Wang, K.; He, T.; Adidharma, H.; Fan, M., Extraction of lithium with functionalized lithium ion-sieves. *Progress in Materials Science* **2016,** *84*, 276-313.
27. Wu, L.; Zhang, C.; Kim, S.; Hatton, T. A.; Mod, H.; Waite, T. D., Lithium

609 recovery using electrochemical technologies: Advances and challenges. *Water*
610 *Research* **2022,** *221*, 118822.
611 28. Battistel, A.; Palagonia, M. S.; Brogioli, D.; La Mantia, F.; Trócoli, R.,
612 Electrochemical Methods for Lithium Recovery: A Comprehensive and Critical Review.
613 *Advanced Materials* **2020,** *32* (23).
614 29. Xu, S.; Song, J.; Bi, Q.; Chen, Q.; Zhang, W.-M.; Qian, Z.; Zhang, L.;
615 Xu, S.; Tang, N.; He, T., Extraction of lithium from Chinese salt-lake brines by
616 membranes: Design and practice. *Journal of Membrane Science* **2021,** *635*, 119441.
617 30. Zhang, Y.; Wang, L.; Sun, W.; Hu, Y.; Tang, H., Membrane technologies for
618 Li^{+}/Mg^{2+} separation from salt-lake brines and seawater: A comprehensive review.
619 *Journal of Industrial and Engineering Chemistry* **2020,** *81*, 7-23.
620 31. Zante, G.; Tr´ebouet, D.; Boltoeva, M., Solvent extraction of lithium from
621 simulated shale gas produced water with a bifunctional ionic liquid. *Applied*
622 *Geochemistry* **2020,** *123*, 104783.
623 32. Jang, E.; Jang, Y.; Chung, E., Lithium recovery from shale gas produced water
624 using solvent extraction. *Applied Geochemistry* **2017,** *78*, 343-350.
625 33. Tian, L.; Liu, Y.; Tang, P.; Yang, Y.; Wang, X.; Chen, T.; Bai, Y.;
626 Tiraferri, A.; Liu, B., Lithium extraction from shale gas flowback and produced water
627 using $H_{1.33}Mn_{1.67}O_4$ adsorbent. *Resources, Conservation & Recycling* **2022,** *185*,
628 106476.
629 34. Zandvakili, S.; Ranjbar, M., Preparation and characterisation of lithium ion
630 exchange composite for the recovery of lithium from brine. *Mineral Processing and*
631 *Extractive Metallurgy* **2018,** *127* (3), 176-181.
632 35. Sun, S.-Y.; Cai, L.-J.; Nie, X.-Y.; Song, X.; Yu, J.-G., Separation of
633 magnesium and lithium from brine using a Desal nanofiltration membrane. *Journal of*
634 *Water Process Engineering* **2015,** *7*, 210-217.
635 36. Xu, P.; Hong, J.; Qian, X.; Xu, Z.; Xia, H.; Tao, X.; Xu, Z.; Ni, Q.-Q.,
636 Materials for lithium recovery from salt lake brine. *Journal of Materials Science* **2021,**
637 *56* (1), 16-63.
638 37. Usov, A. I., Alginic acids and alginates: analytical methods used for their estimation
639 and characterisation of composition and primary structure. *Russian Chemical Reviews*
640 **1999,** *68* (11), 957-966.
641 38. Lentz, L.; Mayer, D. A.; Dogenski, M.; Ferreira, S. R. S., Hybrid aerogels of
642 sodium alginate/graphene oxide as efficient adsorbents for wastewater treatment.
643 *Materials Chemistry and Physics* **2022,** *283*, 125981.
644 39. Song, D.; Park, S.-J.; Kang, H. W.; Park, S. B.; Han, J.-I., Recovery of
645 Lithium(I), Strontium(II), and Lanthanum(III) Using Ca–Alginate Beads. *Journal of*
646 *Chemical & Engineering Data* **2013,** *58* (9), 2455-2464.
647 40. Hong, H. J.; Park, I. S.; Ryu, T.; Ryu, J.; Kim, B. G.; Chung, K. S.,
648 Granulation of Li1.33Mn1.67O4 (LMO) through the use of cross-linked chitosan for
649 the effective recovery of Li+ from seawater. *Chemical Engineering Journal* **2013,** *234*,
650 16-22.

41. Foo, K. Y.; Hameed, B. H., Insights into the modeling of adsorption isotherm systems. *Chemical Engineering Journal* **2010,** *156* (1), 2-10.
42. Rangabhashiyam, S.; Anu, N.; Giri Nandagopal, M. S.; Selvaraju, N., Relevance of isotherm models in biosorption of pollutants by agricultural byproducts. *Journal of Environmental Chemical Engineering* **2014,** *2* (1), 398-414.
43. Tang, S.; Yang, J.; Lin, L.; Peng, K.; Chen, Y.; Jin, S.; Yao, W., Construction of physically crosslinked chitosan/sodium alginate/calcium ion double-network hydrogel and its application to heavy metal ions removal. *Chemical Engineering Journal* **2020,** *393*, 124728.
44. Thommes, M.; Kaneko, K.; Neimark, A. V.; Olivier, J. P.; Rodriguez-Reinoso, F.; Rouquerol, J.; Sing, K. S. W., Physisorption of gases, with special reference to the evaluation of surface area and pore size distribution (IUPAC Technical Report). *Pure and Applied Chemistry* **2015,** *87* (9-10), 1051-1069.
45. Guo, Y.; Bae, J.; Fang, Z.; Li, P.; Zhao, F.; Yu, G., Hydrogels and Hydrogel-Derived Materials for Energy and Water Sustainability. *Chemical Reviews* **2020,** *120* (15), 7642-7707.
46. Alhujaily, A.; Mao, Y. Z.; Zhang, J. L.; Ifthikar, J.; Zhang, X. Y.; Ma, F. Y., Facile fabrication of Mg-Fe-biochar adsorbent derived from spent mushroom waste for phosphate removal. *Journal of the Taiwan Institute of Chemical Engineers* **2020,** *117*, 75-85.
47. Chitrakar, R.; Kanoh, H.; Miyai, Y.; Ooi, K., Recovery of Lithium Ions from Seawater Using a Continuous Flow Adsorption Column Packed with Granulated Chitosan Lithium Manganese Oxide. *Industrial & Engineering Chemistry Research* **2016,** *55* (26), 7218-7225.
48. Park, H.; Singhal, N.; Jho, E. H., Lithium sorption properties of HMnO in seawater and wastewater. *Water Research* **2015,** *87*, 320-7.
49. Liang, J.; Xie, T.; Liu, Y.; Wu, Q.; Bai, Y.; Liu, B., Granular activated carbon (GAC) fixed bed adsorption combined with ultrafiltration for shale gas wastewater internal reuse. *Environmental Research* **2022,** *212* (Pt D), 113486.
50. Ho, Y.; Mckay, G., Pseudo-second order model for sorption processes. *Process Biochemistry* **1999,** *34* (5), 451-465.
51. Qiu, Z.; Wang, M.; Chen, Y.; Zhang, T.; Yang, D.; Qiu, F., Li4Mn5O12 doped cellulose acetate membrane with low Mn loss and high stability for enhancing lithium extraction from seawater. *Desalination* **2021,** *506*, 115003.
52. Tang, L.; Huang, S.; Yan Wang, D. L.; Li, Y.; Li, J.; Wang, Y.; Xie, Y.; Wang, W., Highly Efficient, Stable, and Recyclable Hydrogen Manganese Oxide/Cellulose Film for the Extraction of Lithium from Seawater. *ACS Appled Materials Interfaces* **2020,** *12* (8), 9775-9781.
53. Lai, X.; Yuan, Y.; Chen, Z.; Peng, J.; Sun, H.; Zhong, H., Adsorption-Desorption Properties of Granular EP/HMO Composite and Its Application in Lithium Recovery from Brine. *Industrial & Engineering Chemistry Research* **2020,** *59* (16), 7913-7925.

693 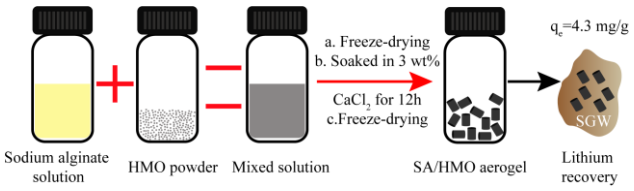

694 **For Table of Contents Use Only.** SA/HMO composite granular adsorbent was
695 prepared by crosslinking method to extract lithium efficiently from shale gas
696 wastewater.

697

698

699